Accepted Manuscript

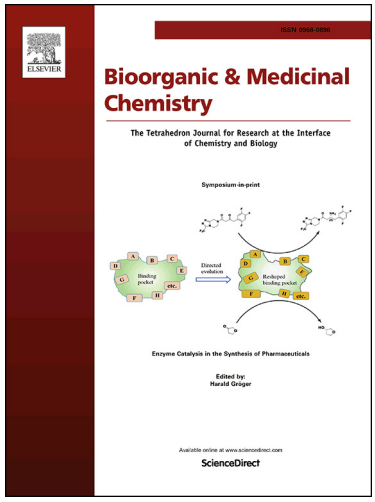

The Parmodulin NRD-21 is an Allosteric Inhibitor of PAR1 Gq Signaling with Improved Anti-Inflammatory Activity and Stability

Disha M. Gandhi, Ricardo Rosas Jr, Eric Greve, Kaitlin M. Kentala, N'Guessan D.-R. Diby, Vladyslava A. Snyder, Allison Stephans, Teresa H.W. Yeung, Saravanan Subramaniam, Elliot DiMilo, Khia E. Kurtenbach, Leggy A. Arnold, Hartmut Weiler, Chris Dockendorff

PII: S0968-0896(19)30527-9
DOI: https://doi.org/10.1016/j.bmc.2019.06.043
Reference: BMC 14980

To appear in: *Bioorganic & Medicinal Chemistry*

Received Date: 13 April 2019
Revised Date: 19 June 2019
Accepted Date: 27 June 2019

Please cite this article as: Gandhi, D.M., Rosas, R. Jr, Greve, E., Kentala, K.M., D.-R. Diby, N., Snyder, V.A., Stephans, A., Yeung, T.H.W., Subramaniam, S., DiMilo, E., Kurtenbach, K.E., Arnold, L.A., Weiler, H., Dockendorff, C., The Parmodulin NRD-21 is an Allosteric Inhibitor of PAR1 Gq Signaling with Improved Anti-Inflammatory Activity and Stability, *Bioorganic & Medicinal Chemistry* (2019), doi: https://doi.org/10.1016/j.bmc.2019.06.043

The Parmodulin NRD-21 is an Allosteric Inhibitor of PAR1 Gq Signaling with Improved Anti-Inflammatory Activity and Stability

Disha M. Gandhi,[†,§] Ricardo Rosas, Jr.,[†,§] Eric Greve,[†] Kaitlin M. Kentala,[†] N'Guessan D.-R. Diby,[†] Vladyslava A. Snyder,[†] Allison Stephans,[†] Teresa H. W. Yeung,[†] Saravanan Subramaniam,[Δ] Elliot DiMilo,[‡] Khia E. Kurtenbach,[†] Leggy A. Arnold,[‡] Hartmut Weiler,[Δ,£] and Chris Dockendorff*[,†]

[†]Department of Chemistry, Marquette University, P.O. Box 1881, Milwaukee, WI, 53201-1881, USA

[‡]Department of Chemistry and Biochemistry, Milwaukee Institute for Drug Discovery, University of Wisconsin, Milwaukee, WI, 53211, USA

[Δ]Blood Research Institute, Versiti, Milwaukee, WI, 53226, USA

[£]Department of Physiology, Medical College of Wisconsin, Milwaukee, WI, 53226, USA

[§] These authors contributed equally to this manuscript.

KEYWORDS: parmodulin, NRD-21, ML161, PAR1, allosteric inhibitor, oxazole, anti-platelet, antithrombotic, anti-inflammatory, biased ligand

ABSTRACT: Novel analogs of the allosteric, biased PAR1 ligand ML161 (parmodulin 2, PM2) were prepared in order to identify potential anti-thrombotic and anti-inflammatory compounds of the parmodulin class with improved properties. Investigations of structure-activity relationships of the western portion of the 1,3-diaminobenzene scaffold were performed using an intracellular calcium mobilization assay with endothelial cells, and several heterocycles were identified that inhibited PAR1 at sub-micromolar concentrations. The oxazole NRD-21 was profiled in additional detail, and it was confirmed to act as a selective, reversible, negative allosteric modulator of PAR1. In addition to inhibiting human platelet aggregation, it showed superior anti-inflammatory activity to ML161 in a qPCR assay measuring the expression of tissue factor in response to the cytokine TNF-alpha in endothelial cells. Additionally, NRD-21 is much more plasma stable than ML161, and is a promising lead compound for the parmodulin class for anti-thrombotic and anti-inflammatory indications.

1. INTRODUCTION

The use of biased ligands for G protein coupled receptors (GPCRs) has emerged as a promising strategy for maximizing therapeutic signals mediated by GPCRs, while potentially mitigating undesired side effects linked to alternative signaling pathways initiated by the same receptors. Protease-activated receptors (PARs) are GPCRs that are activated by a variety of vascular proteases that cleave the N-termini of PARs, revealing a tethered peptide that activates the receptor[1] and initiates a plethora of signals.[2] PARs are present in a variety of tissues and are implicated in a variety of pathologies including thrombosis, inflammation, and cancer cell metastasis.[3,4] The varied phenotypic effects of PAR activation have recently been connected to the activation of specific G-proteins and arrestins,[5] and biased signals have been observed with proteases such as activated protein C (aPC) that cleave PAR N-termini at alternative sites.[6-10] Synthetic peptides[11,12] and peptidomimetics[13,14] based on PAR tethered ligands have also shown biased signaling by blocking or activating only a subset of signals. Pepducins, a novel class of fatty acid-tethered peptides modeled after intracellular

GPCR loops developed by Kuliopulos and coworkers,[15-17] have been reported to act as biased antagonists at PAR2.[4,18] Previously, we reported that small molecules identified via high-throughput screening (HTS) are capable of inhibiting platelet granule secretion, while permitting the shape change of platelets normally observed upon platelet activation via PAR1 agonism, thus acting as "biased antagonists" of PAR1.[19,20] Our collaborators (Flaumenhaft and coworkers) have accrued evidence that these small molecules, termed parmodulins, act at the intracellular side of PAR1 to block signaling mediated by Gq, but not G12/13.[21,22] The parmodulin ML161 (**1**, also referred to as parmodulin 2 or PM2, Figure 1) was found to promote cytoprotective and anti-inflammatory effects in endothelium in a manner similar to aPC,[22] and as with aPC it was highly effective at minimizing necrosis of coronary tissue in a mouse model of myocardial infarction (MI).[23] We also recently confirmed that ML161 and its aniline analog RR-90 are selective, reversible, and allosteric inhibitors (negative allosteric modulators) of PAR1 signaling via the G protein Gq.[24] The presence of PAR1 is required for the cytoprotective effects of aPC[25] and ML161[21,22] in endothelium, and targeting PAR1 with parmodulins to inhibit pro-inflammatory or pro-thrombotic signals while activating beneficial anti-inflammatory and/or cytoprotective signals could be an effective therapeutic strategy for sepsis, stroke, and thrombosis. This manuscript describes our efforts to more deeply explore structure-activity relationships (SARs) at the western side of parmodulins possessing the 1,3-diaminobenzene scaffold, exemplified by ML161.

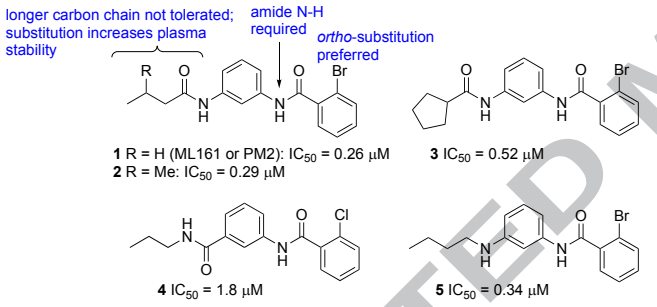

Figure 1. Previous parmodulins and their performance in a platelet P-selectin assay.[20]

ML161 was previously assigned as a Molecular Libraries probe,[20,26] and was our most potent analog to date in the P-selectin assay, a flow cytometry assay which measures levels of P-selectin on the surface of activated platelets. Our interest in measuring the effects of parmodulins in endothelial cells led us to develop a protocol for an intramolecular calcium mobilization (iCa^{2+}) assay using adherent EA.hy926 cells in 96 well plates.[24] Both responses are driven by PAR1 Gq, but the endothelial calcium assay also offers higher throughput and lower variability than the platelet P-selectin assay, so we have utilized it as our primary assay for ongoing studies. Compounds were screened in 96 well plates at a concentration of 10 μM, using the PAR1 tethered ligand peptide TFLLRN (5 μM) as agonist. 7-point concentration-response curves were obtained for compounds demonstrating >70% inhibition in this screen, which was an arbitrary cutoff.

Scheme 1. General conditions for the synthesis of western amide analogs.

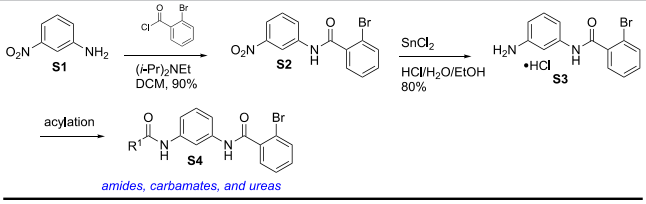

A significant liability of ML161 is its low stability in mouse plasma. The branched amide **2** was equipotent to ML161 in the platelet P-selectin assay, but showed greatly improved stability in mouse plasma after 5 h (65% remaining vs 2%), presumably due to increased resistance to protease-catalyzed hydrolysis.[20] Unfortunately, **2** possesses decreased solubility in water with 1% DMSO (9 μM vs 58 μM for **1**),[20] and mediocre inhibition in the endothelial *i*Ca^{2+} assay (Table 1).[24] Therefore, we focused our efforts on finding alternative analogs that could offer equal or better potency than ML161 in the *i*Ca^{2+} assay but with improved plasma stability, which is particularly important for longer duration in vivo experiments.

2. RESULTS

This manuscript describes our SAR studies with modifications to the "western" end of the scaffold. Many of these analogs, including the most promising analogs identified herein, could be prepared via simple acylation reactions of aniline precursors (Scheme 1). The eastern 2-bromobenzamide of ML161 that was optimized previously was fixed at this stage, though other eastern benzene substitutions are also tolerated.

Table 1. SAR of simple alkyl analogs

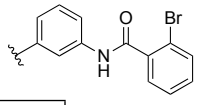

Cmpd; ID#	Structure	*i*Ca^{2+} assay %Inhib; pIC_{50}[a]	Cmpd; ID#	Structure	*i*Ca^{2+} assay %Inhib; pIC_{50}[a]
1 ML161	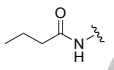	82±2% 6.1±0.1	**8** EMG-21		54±3% 5.5±0.3
2 CJD-125	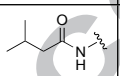	82±2% undef.[b]	**9** NRD-25	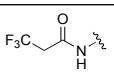	88±1% 6.4±0.2
3 EMG-22	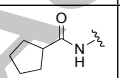	65±2%	**10** EMG-23	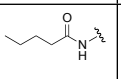	23±5%[d]
6 CJD-159	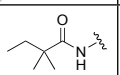	21%[c]	**11** RR-10	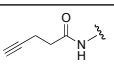	79% 4.0±5.1
7 AS-1	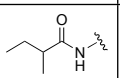	27±6%	**12** RR-71	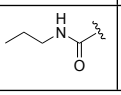	63±4% 6.7±0.2

[a]Assays were performed with adherent EA.hy926 endothelial cells according to the protocol reported in the Supporting Info. % Inhibition was measured at 10 μM with 5 μM TFLLRN-NH_2 and n = 4 wells, unless otherwise noted, with standard error of the mean (SEM) provided. pIC_{50}s (–logIC_{50}s) were estimated from curves fitted to measurements on 3 separate wells for each concentration, using

4-variable non-linear regression in GraphPad Prism v. 6. The detailed assay protocol was previously described.[24] [b]IC_{50} is undefined– a double sigmoidal concentration-response curve was not obtained. [c]In platelet P-selectin assay.[20] [d]n = 3.

Following up on our previous modifications at the western side exemplified by **1** and **2**, we explored the role of branching and chain length (Table 1). The cyclopentyl analog **3** showed moderate inhibition, but increasing further the level of substitution at the alpha position (**6**) greatly increased plasma stability but decreased inhibition greatly in the platelet P-selectin assay.[20] The acyclic analog **7** also showed weak efficacy in the *i*Ca^{2+} assay. Compound **8**, with one carbon less than ML161, also showed decreased activity, but interestingly its more lipophilic trifluoromethyl analog **9** showed increased potency (IC_{50} = 0.38 μM) compared to **8** and similar activity to ML161. Alternatively, extension of the carbon chain of ML161 by one led to decreased efficacy and/or potency (compounds **10** and **11**), which is consistent with what we observed previously with platelets.[20] A close analog of the previously-reported reverse amide **4** (Figure 1) was also prepared (**12**), and showed very good potency (IC_{50} = 0.22 μM), but only moderate efficacy (~50% maximal inhibition). Such reverse amides could address potential liabilities associated with toxic anilide or aniline hydrolysis products.[27]

Introduction of polar functional groups was performed in order to improve the potency and drug-like properties of **1** and **2** (Table 2). Addition of hydroxy or methoxy groups (compounds **13**–**18**) led to significant losses of efficacy. Malonate derivatives (**19**–**21**) also showed weak efficacy. Two carbamates were synthesized (**22** and **23**), with **23** showing moderate activity (60% inhibition at 10 μM), as did ether **24**.

Table 2. SAR of neutral or acidic analogs

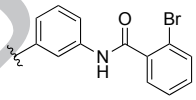

Cmpd; ID#	Structure	*i*Ca^{2+} assay %Inhib; pIC_{50}[a]	Cmpd; ID#	Structure	*i*Ca^{2+} assay %Inhib; pIC_{50}[a]
13 NRD-26	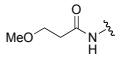	39±5%	**19** DG-14	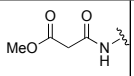	11±12%
14 DG-119	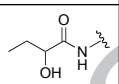	21±2%	**20** DG-17	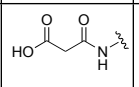	37±11%
15 DG-120	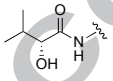	25±5%	**21** DG-37	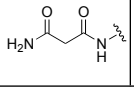	36±13%
16 DG-121	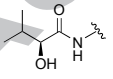	48±13%	**22** VAK-9	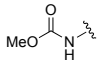	42±12%
17 VAK-12	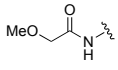	38±5%	**23** VAK-10	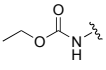	60±4%
18 RR-72	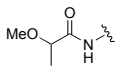	58±7%	**24** TY-13	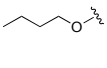	57±4%

[a]Assays were performed with adherent EA.hy926 endothelial cells according to the protocol reported in the Supporting Info. % Inhibition was measured at 10 μM with 5 μM TFLLRN-NH_2 and n = 4 wells, unless otherwise noted, with standard error of the mean (SEM) provided. pIC_{50}s (–logIC_{50}s) were estimated from curves fitted to measurements on 3 separate wells for each concentration, using 4-variable non-linear regression in GraphPad Prism v. 6. The detailed assay protocol was previously described.[24]

Continuing with more basic amine functionality (Table 3), we found that incorporation of a dimethylamine unit at the western end (**25**) led to a complete loss of activity. However, as previously reported,[20,24] the aniline RR-90 (**5**) showed very good activity and similar potency to ML161. As with the amide series of Table 1, removal of a carbon from the aniline chain (**26**) decreased activity, as did the introduction of an oxygen atom (ether **27**). Preparation of the more basic analog **28** also led to a steep drop in efficacy. Interestingly, the anilines **29** and **30** both showed evidence of activation, rather than inhibition, of PAR1. Aniline **29** was synthesized via a reductive amination reaction with the aniline precursor **S3** (Scheme 1) and cyclopentenone, and **30** was prepared by cyclization of the same precursor with 1,4-dibromobutane. Aniline **30** is presently under investigation as a potential positive allosteric modulator of PAR1.

Next, we explored heterocyclic amide analogs (Table 4). The exploration of western pyrrolidine derivatives (**27**–**31**) initially yielded differences in activity between the *R*- and *S*-enantiomers in both the Boc-protected pyrrolidines (**31**, **33**) and the deprotected derivatives (**32**, **34**). However, re-synthesis and retesting of **31**–**34** to obtain concentration-response curves did not show significant inhibition of calcium mobilization by the PAR1 agonist TFLLRN-NH_2.

Table 3. SAR of amine analogs

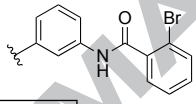

Cmpd; ID#	Structure	*i*Ca^{2+} assay %Inhib; pIC_{50}[a]	Cmpd; ID#	Structure	*i*Ca^{2+} assay %Inhib; pIC_{50}[a]
25 VAK-11	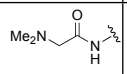	3±3%	**28** DG-75	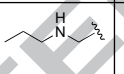	17±6%
5 RR-90	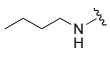	85±2% 6.0±0.2	**29** KMK-18		–12±6%
26 KMK-22		13±2%	**30** KMK-17		–60±8%
27 TY-14	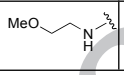	43±6%[b]			

[a]Assays were performed with adherent EA.hy926 endothelial cells according to the protocol reported in the Supporting Info. % Inhibition was measured at 10 μM with 5 μM TFLLRN-NH_2 and n = 4 wells, unless otherwise noted, with standard error of the mean (SEM) provided. pIC_{50}s ($-\log IC_{50}$s) were estimated from curves fitted to measurements on 3 separate wells for each concentration, using 4-variable non-linear regression in GraphPad Prism v. 6. The detailed assay protocol was previously described.[24] [b]n = 3.

The furan **35** showed a high level of inhibition (92%, IC_{50} = 0.32 μM), which prompted us to explore other oxygen-containing heterocycles, particularly since monosubstituted furans such **35** may suffer from undesirable oxidative metabolism.[28] The tetrahydrofurans **36** and **37** showed only modest inhibition, but the oxazoles **38** and **39** showed very good inhibition. The phenyl analog **40** can be considered as a control compound, and it displayed moderate inhibition (58%).

The potent oxazoles **38** (NRD-21) and **39** (NRD-23) were profiled further, along with the trifluoromethyl analog **9** (NRD-25) and the furan **35** (VAK-7) (Figure 2). Concentration-response curves were obtained in our intracellular calcium mobilization (*i*Ca^{2+})

assay. All four analogs showed similar potencies (IC_{50} = 0.32 to 0.42 μM), though interestingly the oxazole **38** showed much better efficacy than **39**, which only inhibited calcium activity at ~50% at the highest concentration (31.6 μM).

Our previous studies showed the lead compound ML161 (**1**) and aniline **5** to have selective and reversible activity towards PAR1. We endeavored to determine if our novel analogs possess the same properties. Selectivity for PAR1 was conducted with our calcium mobilization assay and PAR1 or PAR2 agonists (Figure 3). Ea.hy926 cells were dosed with either vorapaxar at 0.316 μM or the selected parmodulin at 10 μM. The cells were then stimulated using either the PAR1 agonist TFLLRN-NH_2 or the PAR2 agonist SLIGKV-NH_2 at 3.16 μM. All parmodulins and vorapaxar showed inhibition of the PAR1 receptor (Figure 3A). Consistent with Table 4, oxazole **39** was the only parmodulin that showed less than 75% inhibition of PAR1, while all other parmodulins and vorapaxar exhibited >75% inhibition (<25% stimulation) (Figure 3A). All antagonists tested with the PAR2 agonist SLIGKV-NH_2 showed no inhibition of PAR2 (Figure 3B), therefore we conclude that all analogs are highly selective for PAR1 over PAR2.

Table 4. SAR of heterocyclic amide analogs

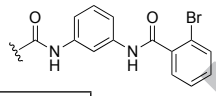

Cmpd; ID#	Structure	*i*Ca^{2+} assay %Inhib; pIC_{50}[a]	Cmpd; ID#	Structure	*i*Ca^{2+} assay %Inhib; pIC_{50}[a]
31 KMK-14A		65±4%[b]	**36** AS-2		42±3%
32 KMK-14B		63±4%[b]	**37** AS-4		44±2%
33 KMK-15A		–8±6%[b]	**38** NRD-21		90±1% 6.3±0.1
34 KMK-15B		4±6%[b]	**39** NRD-23		82±1% 6.4±0.1
35 VAK-7		92±1% 6.5±0.2	**40** NRD-22		58±4%

[a]Assays were performed with adherent EA.hy926 endothelial cells according to the protocol reported in the Supporting Info. % Inhibition was measured at 10 μM with 5 μM TFLLRN-NH_2 and n = 4 wells, unless otherwise noted, with standard error of the mean (SEM) provided. pIC_{50}s (–logIC_{50}s) were estimated from curves fitted to measurements on 3 separate wells for each concentration, using 4-variable non-linear regression in GraphPad Prism v. 6. The detailed assay protocol was previously described.[24] [b]These compounds were resynthesized and retested and were found to be inactive when 7-point concentration-response curves were obtained.

We also conducted "wash" studies where the endothelial cells were treated with select inhibitors, then washed twice with buffer prior to addition of the agonist and measurement of intracellular calcium levels (Figure 4).[26] Parmodulins were compared to vorapaxar which is a known poorly reversible orthosteric inhibitor. As expected, all parmodulins tested had a significant loss of inhibition after washing, while vorapaxar remained unaffected, confirming that they inhibit PAR1 in a reversible manner.

Out of the four parmodulins profiled, compound **38** (NRD-21) was selected for further studies; we reasoned that the trifluoromethyl analog **9**, though potent, likely possesses the same plasma stability and solubility liabilities as ML161. ML161 was characterized as a negative allosteric modulator in both platelets and endothelial cells in our previous studies, and we reasoned that

the structurally similar NRD-21 would act in a similar manner. Indeed, increasing concentrations of antagonist **38** led to a reduction in efficacy of the PAR1 agonist TFLLRN-NH_2 (Figure 5). The reduction of maximum efficacy ("ceiling effect") of the PAR1 agonist in the presence of NRD-21, rather than the simple rightward shift in concentration-response curves, is consistent with the action of NRD-21 as a negative allosteric modulator of TFLLRN-NH_2 at PAR1, rather than a simple competitive inhibition. We previously reported this phenomenon with ML161.[20,24] Interestingly the drop in maximal efficacy is not as pronounced for NRD-21 as for the aniline **5** (RR-90), which we previously described.[24]

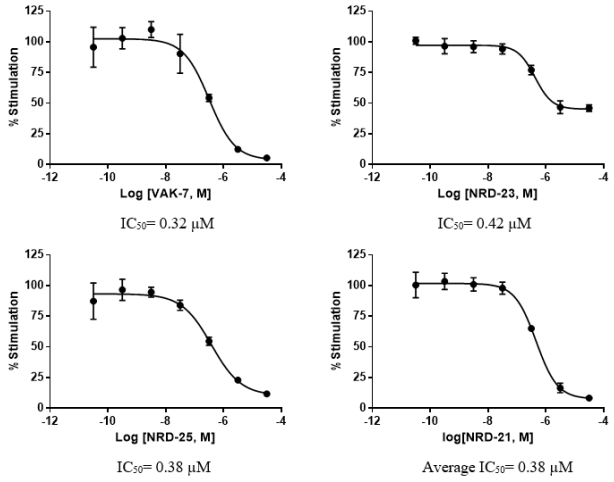

Figure 2. Concentration-response curves for PAR1 antagonists in the TFLLRN-NH_2-mediated (5 µM) iCa^{2+} mobilization assay with Ea.hy926 cells: A) **35** (VAK-7), B) **39** (NRD-23), C) **9** (NRD-25), D) **38** (NRD-21).

Next, an assay was performed to measure the ability of NRD-21 to inhibit platelet aggregation. PAR1 is highly expressed in platelets, and its activation leads to aggregation and coagulation. The platelet aggregation assay was performed with ML161 and NRD-21 (Figure 4). In both cases, human washed platelets were incubated with parmodulins at 10 µM, then the PAR1/2 agonist SFLLRN-NH_2 (1.5 µM) was added. (Figure 6). Complete inhibition of platelet aggregation by both ML161 and NRD-21 was observed.

The anti-inflammatory and cytoprotective effects reported for ML161[21-23] begged the question if other structurally related parmodulins also share these effects. To this end, we performed a qPCR assay measuring the expression of tissue factor (TF) in endothelial cells (HUVEC) in response to the inflammatory cytokine Tumor Necrosis Factor-alpha (TNF-α). TF has been long established to mediate the pro-inflammatory and pro-coagulant effects[27] of TNF-α[28,29] and endotoxins,[30] and unnatural TF expression is therefore the driver of disseminated intravascular coagulation (DIC) observed under conditions of cancer or sepsis.[31] We measured the level of TF mRNA 4 h after treatment with ML161 or NRD-21 followed by the addition of TNF-α (Figure 7). Pretreatment with ML161 (column 4) blocked the ~3-fold increase in TF expression caused by TNF-α alone (column 1), and NRD-21 was even more efficacious, dropping TF RNA levels to below baseline levels. The mechanism of this decrease in TF expression has yet to be delineated, but is presently under investigation.

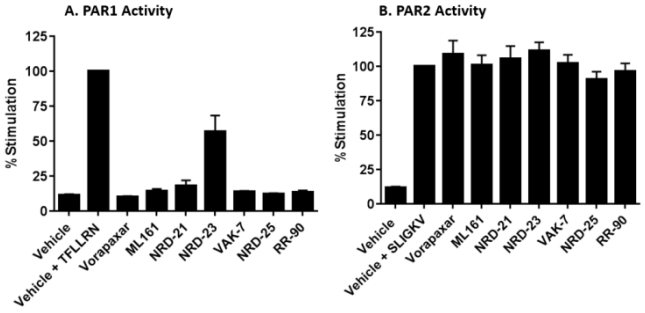

Figure 3. Selectivity data of antagonists in A) PAR1 (TFLLRN-NH_2)- and B) PAR2 (SLIGKV-NH_2)-driven iCa^{2+} mobilization. Parmodulins were used at 10 µM; vorapaxar was used at 0.316 µM. PAR1 agonist TFLLRN-NH_2 and PAR2 agonist SLIGKV-NH_2 were used at 3.16 µM; Vehicle (V) = 10% DMSO/water.

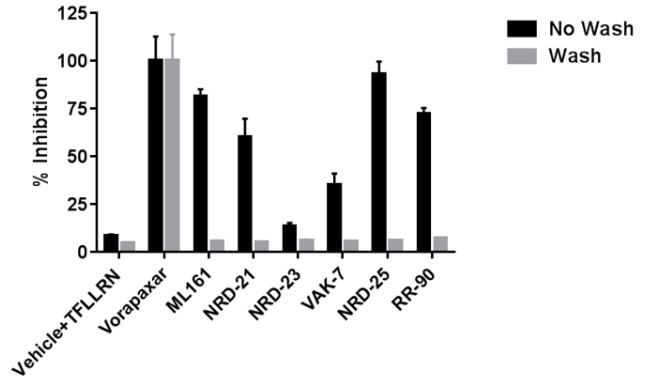

Figure 4. Reversibility studies of the PAR1 antagonist vorapaxar and selected parmodulins. Parmodulins were used at 10 µM; vorapaxar was used at 0.316 µM. PAR1 agonist TFLLRN-NH_2 and PAR2 agonist SLIGKV-NH_2 were used at 3.16 µM; Vehicle (V)= 10% DMSO/water. Cells containing antagonist were washed with buffer prior to the treatment with PAR1 agonist TFLLRN-NH_2 (5 µM).

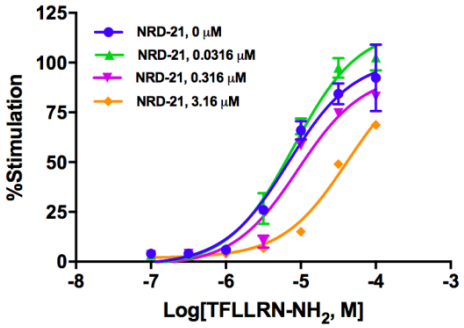

Figure 5. iCa^{2+} concentration-response of the PAR1 agonist TFLLRN-NH_2 in the presence of increasing concentrations of NRD-21.

With these promising results in hand with NRD-21, we measured its stability and a number of parameters relevant to its use as an *in vivo* probe (Table 5). Importantly, NRD-21 is much more plasma stable than ML161. After 4 h in mouse plasma, ~32% of NRD-21 remained, while ML161 was less than 1%. Improved stability in human plasma was also observed for NRD-21 (97% vs 79% after 4 h), as shown in Figure 8. As with ML161, NRD-21 also shows excellent stability in the presence of human liver microsomes, with no apparent degradation after 1 h. It also shows no measurable toxicity in a human cell line (hepG2). An area for improvement remains the low solubility of the current lead compounds of this class, with a solubility of 17 µM for NRD-21 in a kinetic aqueous solubility assay with 2.5% DMSO. Both compounds were also profiled for off-target receptor binding by the

Psychoactive Drug Screening Program (PDSP).[32] Both modified radioligand binding to 3 or 4 different targets, including inhibition of binding to the peripheral benzodiazepine receptor (PBR) and activation of the serotonin transporter (SERT).

Figure 6. Human platelet aggregation assay of A) ML161 (10 μM, red trace) and B) NRD-21 (10 μM, red trace) in the presence of the PAR1/2 agonist SFLLRN-NH_2 (1.5 μM). Blue traces = DMSO.

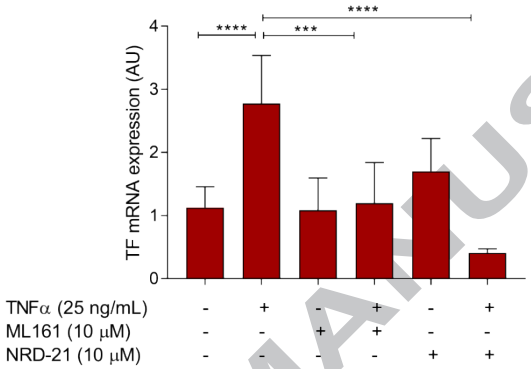

Figure 7. qPCR assay (n = 3) measuring the inhibition of TNF-α (25 ng/mL) induced TF expression in HUVEC after treatment with ML161 and NRD-21 (10 μM). Inhibitors were added at t = 0, TNF-α was added at t = 1 h, and mRNA was measured at t = 4 h. Data was analyzed with one-way ANOVA followed by Bonferroni's multiple comparisons test. *P<0.05, **P<0.01, ***P<0.001, ****P<0.0001.

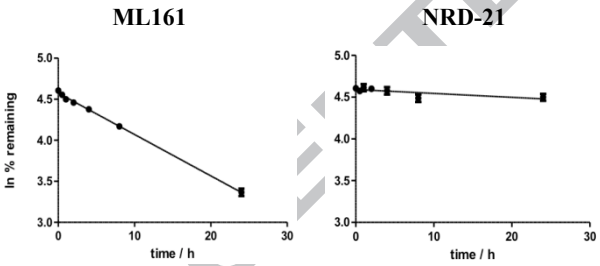

Figure 8. Plasma stability of ML161 (left) and NRD-21 (right). Points indicate the natural logarithm of the average of 3 replicates at each time point.

3. DISCUSSION

Our SAR studies at the western end of the 1,3-diaminobenzene scaffold have determined that lipophilic groups of limited size are best able to inhibit PAR1-driven Gq signaling. However, some heteroatom functionality is tolerated, with western heterocycles giving the most promising profiles. The oxazole NRD-21 was identified as a compound with slightly improved potency over our previous lead compound ML161, but with much improved plasma stability, making it more suitable for in vivo studies.

Most notably, NRD-21 is highly efficacious in the inhibition of TNF-α-mediated TF expression in endothelium, making it a promising lead within this new class of parmodulin anti-inflammatory agents. The signaling pathway(s) leading to the anti-inflammatory effects of the parmodulins is not fully understood, but Flaumenhaft has published evidence consistent with a PAR1-mediated (via Gβγ) signaling pathway that ultimately drives transcriptional responses.[22] Conversely, the FDA-approved orthosteric PAR1 antagonist vorapaxar has shown deleterious effects in cultured endothelium, including increased levels of apoptosis and decreased barrier integrity.[21] We have also demonstrated, here and previously,[21,24] that unlike vorapaxar, parmodulins are readily reversible inhibitors of PAR1, which is an important safety consideration for anti-thrombotic agents. NRD-21 also inhibited human platelet aggregation similarly to ML161. We conclude that the parmodulin class of intracellular allosteric ligands of PAR1, exemplified by NRD-21 with its 1,3-diaminobenzene scaffold, is promising for both anti-thrombotic and anti-inflammatory-related indications. Efforts are ongoing to identify additional potent parmodulins, characterize their signaling pathway(s), and further investigate their utility in thrombosis and inflammation-related and proliferative disorders.

Table 5. Comparison of ML161 and NRD-21

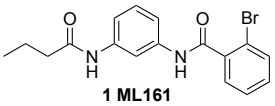

1 ML161

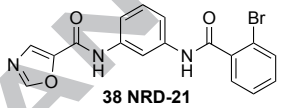

38 NRD-21

	ML161	**NRD-21**
PAR1 iCa^{2+} assay[a] Average IC_{50} ± SEM	0.57 ± 0.08 μM (n = 10)	0.37 ± 0.13 μM (n = 6)
Plasma stability	<1% (4 h, mouse) 79% (4 h, human)	32% (4 h, mouse) 97% (4 h, human)
Microsomal stability	99% (1 h, human)	99% (1 h, human)
Kinetic aqueous solubility (2.5% DMSO)	24 μM	17 μM
PAR2 activity?	None observed	None observed
Off-target effects[b]	4: Beta1 = 49%; Beta3 = 32%; PBR = 84%; SERT = –44%	3: 5HT-5A = –31%; NET = 31%; PBR = 67%; SERT = –44%
Cytotoxicity (CC_{50}) (human hepG2 cells)	>150 μM	>150 μM
Reversible?	Yes	Yes

[a]Average of independent assays, each with IC_{50}s determined from curve fits with n = 3. See e.g. Table 1 for more details. [b]Fraction of off-targets for which there is >20% inhibition (at 10 μM concentration) of 41 targets from the Psychoactive Drug Screening Program. [b]Number of off-targets (out of 44) for which there is >30% inhibition or activation of standard radioligand binding (at 10 μM concentration) of 44 targets from the Abbreviations of target names with mean % inhibition of binding are given. 5HT = 5-hydroxytryptamine receptor; Beta = β-adrenoceptor; NET = norepinephrine transporter; PBR = peripheral benzodiazepine receptor (rat); SERT = serotonin transporter. Off-target assays were performed by the National Institute of Health Psychoactive Drug Screening Program (PDSP).

4. EXPERIMENTAL SECTION

4.1 General synthetic information. All reagents and solvents, including anhydrous solvents, were purchased from commercial vendors and used as received. Deionized water was purified by charcoal filtration to a minimum resistance of 15 MΩ and used for reaction workups

and in reactions with water. NMR spectra were recorded on Varian 300 MHz or 400 MHz spectrometers as indicated. Proton and carbon chemical shifts are reported in parts per million (ppm; δ) relative to tetramethylsilane (^{1}H δ 0), or $CDCl_3$ (^{13}C δ 77.16), $(CD_3)_2CO$ (^{1}H δ 2.05, ^{13}C δ 29.84), d_6-DMSO (^{1}H δ 2.50, ^{13}C δ 39.5), or CD_3OD (^{1}H δ 3.31, ^{13}C δ 49.00). NMR data are reported as follows: chemical shifts, multiplicity (obs = obscured, app = apparent, br = broad, s = singlet, d = doublet, t = triplet, q = quartet, m = multiplet, comp = complex overlapping signals); coupling constant(s) in Hz; integration. Unless otherwise indicated, NMR data were collected at 25 °C. Filtration was performed by vacuum using VWR Grade 413 filter paper, unless otherwise noted. Flash chromatography was performed using Biotage SNAP cartridges filled with 40-60 μm silica gel on Biotage Isolera automated chromatography systems with photodiode array UV detectors. Analytical thin layer chromatography (TLC) was performed on Agela Technologies 0.25 mm glass plates with 0.25 mm silica gel. Visualization was accomplished with UV light (254 nm) and $KMnO_4$ stain, unless otherwise noted. Chemical names were generated and select chemical properties were calculated using either ChemAxon Marvin suite or ChemDraw Professional 15.1. NMR data were processed using either MestreNova or ACD/NMR Processor Academic Edition using the JOC report format. High-resolution mass spectra (HRMS) were obtained from the University of Cincinnati Environmental Analysis Service Center using an Agilent 6540 Accurate-Mass LC-MS with Q-TOF.

4.2 LC-MS characterization methods

Tandem liquid chromatography/mass spectrometry (LC-MS) was performed on a Shimadzu LCMS-2020 with autosampler, photodiode array detector, and single-quadrupole MS with ESI and APCI dual ionization using a Peak Scientific nitrogen generator.

Method A
Column: Phenomenex Gemini C_{18} (100 x 4.6 mm, 3 μm particle size, 110 Å pore size)
Column temperature: 40 °C
Sample Injection: 1–5 μL of sample in MeCN or MeOH
Chromatographic monitoring: UV absorbance at 210 or 254 nm
Mobile Phase: Solvent A: H_2O w/ 0.1% formic acid; Solvent B: MeOH w/ 0.1% formic acid
Flow Rate: 1.0 mL/min
Gradient: 0 to 0.1 min: 25% MeOH (Isocratic)
0.1 min to 5 min: 25% to 95% MeOH (Gradient)
5 min to 7 min: 95% MeOH (Isocratic)

Method B
Column: Phenomenex Gemini C_{18} (100 x 4.6 mm, 3 μm particle size, 110 Å pore size)
Column temperature: 40 °C
Sample Injection: 1–5 μL of sample in MeCN or MeOH
Chromatographic monitoring: UV absorbance at 210 or 254 nm
Mobile Phase: Solvent A: H_2O w/ 0.1% formic acid; Solvent B: MeCN w/ 0.1% formic acid
Flow Rate: 1.0 mL/min
Gradient: 0 to 0.1 min: 50% MeCN (Isocratic)
0.1 min to 5 min: 50% to 95% MeCN (Gradient)
5 min to 7 min: 95% MeCN (Isocratic)

Method C
Column: Phenomenex Gemini C_{18} (100 x 4.6 mm, 3 μm particle size, 110 Å pore size)
Column temperature: 40 °C
Sample Injection: 1–5 μL of sample in MeCN or MeOH
Chromatographic monitoring: UV absorbance at 210 or 254 nm
Mobile Phase: Solvent A: H_2O w/ 0.1% formic acid; Solvent B: MeCN w/ 0.1% formic acid
Flow Rate: 1.0 mL/min
Gradient: 0 to 0.5 min: 50% MeCN (Isocratic)
0.5 min to 4 min: 50% to 95% MeCN (Gradient)
4 min to 6.3 min: 95% MeCN (Isocratic)

4.2 General procedures for synthesis of parmodulins via amide coupling.

Method A: Amide coupling using EDC. To a round bottom flask with stir bar under nitrogen were added the appropriate carboxylic acid and anhydrous DCM/DMF (85:15; 0.2–0.6 M). The amine HCl salt to be coupled (1.2 eq.), HOBt (1.2 eq.), EDC-HCl (1.2 eq.), and DIPEA (2.1 eq.) were added and the reaction was stirred under nitrogen until complete, as measured by TLC and/or LC-MS. The reaction was diluted with DCM, washed with saturated aq. $NaHCO_3$, 1M aq. HCl, and brine, then dried over Na_2SO_4, filtered, and concentrated under reduced pressure prior to purification by flash chromatography (SiO_2). The following parmodulins were synthesized utilizing this method: **3**, **6**, **8**, **9**, **13**, **17**, **25**, and **35**.

Method B: Conversion to the acid chloride and subsequent acylation. To an oven-dried round bottom flask with stir bar under nitrogen were added the carboxylic acid, dry DCM, and 3Å molecular sieves. Oxalyl chloride (1.2 eq.) and a catalytic amount of DMF (1–2 mol %) were added and the reaction was stirred while attached to a bubbler (to monitor production of CO_2) at 20 °C for 2–3 h. The amine HCl salt (1 eq.) in DCM and DIPEA (2 eq.) were added and the reaction was stirred under nitrogen for 3–6 h. The reaction was diluted with EtOAc and washed with half-saturated aq. $NaHCO_3$, 1M HCl (30 mL), and brine, then dried over Na_2SO_4, filtered, and concentrated under reduced pressure prior to purification by flash chromatography (SiO_2). The following parmodulins were synthesized utilizing this method: **7**, **11**, **18**, and **36**–**40**.

Method C: Acylation. To an oven-dried round bottom flask with stir bar and under nitrogen were added the acid chloride, dry DCM, and 3Å molecular sieves. The amine HCl salt (1 eq.) in DCM and DIPEA (2 eq.) were added and the reaction was stirred under nitrogen for 3–6 h. The reaction was diluted with EtOAc and washed with half-saturated aq. $NaHCO_3$, 1M HCl (30 mL), brine, dried over Na_2SO_4, filtered, and concentrated under reduced pressure to give crude product. The following parmodulins were synthesized utilizing this method: **10**, **12**, **19**, and **24**.

Method D: Amide coupling using HATU. To a round bottom flask with stir bar under nitrogen was added the carboxylic acid and anhydrous DCM. The amine (1.2 eq.), HATU (1.2 eq.), and DIPEA (1.2 eq.) were added and the reaction was stirred under nitrogen. The reaction was diluted with DCM (75 mL) and washed with saturated $NaHCO_3$, 1M HCl (30 mL), brine, dried over Na_2SO_4, filtered, and concentrated under reduced pressure to give crude material. The following parmodulins were synthesized utilizing this method: **14-16**, **31**, and **33**.

4.3 Preparation of *N*-[3-(2-bromobenzamido)phenyl]-1,3-oxazole-5-carboxamide (38, NRD-21, Scheme S1). To a vial with a magnetic stir bar was added aniline **S3** (50.2 mg, 0.173 mmol), oxazole-5-carboxylic acid (27 µL, 0.347 mmol), EDC-HCl (33.9 mg, 0.177 mmol), and HOBt (26.7 mg, 0.174). The vial was sealed and flushed with nitrogen for 5 min., then DCE (1.5 mL) and DMF (0.5 mL) were added. To the resulting solution was added a 10% solution of pyridine in DCE (0.14 mL, 0.173 mmol) by syringe, and the reaction was stirred for 24 h. A sample aliquot was taken from the reaction, concentrated under reduced pressure, dissolved in a minimal amount of HPLC grade MeCN, and analyzed by LC-MS to confirm reaction completion. The reaction was then diluted with EtOAc (30 mL) and washed with half-saturated aq. $NaHCO_3$ (3 x 15 mL), brine (2 x 10 mL), dried over Na_2SO_4, filtered, and concentrated under reduced pressure. The crude product was dissolved in a minimal amount of DCM, loaded onto a 10 g silica gel column, and purified by flash chromatography (MeOH:DCM, 0–8%) to give **38** as a yellow oil (40 mg, 60%). TLC: mobile phase: MeOH:DCM (6:94), R_f = 0.30; LC-MS t_R = 4.29 min. (Characterization Method A); m/z = 387.29 (M + H); ^{1}H NMR (300 MHz, CD_3OD) δ = 8.36 (s, 1 H), 8.15 (t, *J* = 2.0

Hz, 1 H), 7.85 (s, 1 H), 7.64 (dd, *J* = 1.0, 7.9 Hz, 1 H), 7.53 - 7.41 (m, 5 H), 7.41 - 7.28 (m, 3 H); ^{13}C NMR (100 MHz, CD_3OD) δ = 169.1, 157.2, 154.7, 147.0, 140.2, 140.1, 139.3, 134.2, 132.3, 131.2, 130.2, 129.8, 128.7, 120.5, 118.5, 118.1, 114.4. HRMS (ESI^+) calculated for $C_{17}H_{12}BrN_3O_3$ (M+H) 386.0135, found 386.0147.

ASSOCIATED CONTENT

Supporting Information

Assay protocols, additional synthetic protocols, and compound characterization data (^{1}H NMR, ^{13}C NMR, and LC-MS chromatograms) (PDF).

AUTHOR INFORMATION

Corresponding Author

* Email: christopher.dockendorff@mu.edu Tel: 1-414-288-1617.

Author Contributions

D.M.G. and R.R. contributed equally to this manuscript. Conceived project: C.D.; Designed compounds: C.D., D.M.G., R.R.; Synthesized and characterized analogs: D.M.G., R.R., N.D.-R.D., E.G., A.S., K.M.K., T.H.Y.Y., K.E.K.; Performed pharmacology and analyzed data: D.M.G., R.R. C.D.; Performed physicochemical/physiochemical profiling: E.D., L.A.A.; Performed RNA assay and analyzed related data: S.S., H.W; Wrote manuscript: C.D., R.R.; Prepared Supporting Information and edited the manuscript: R.R., D.M.G., C.D., L.A.A., S.S., E.G.

Funding Sources

C.D. thanks the National Heart, Lung, and Blood Institute (NHLBI) (R15HL127636) for support, and Marquette University for startup funding. H.W. and S.S. thank NHLBI for funding (R01HL133348). K.M.K. (Honors Program), D.M.G., and R.R. thank Marquette University for summer support. N.D.-R.D thanks the National Science Foundation (via Milwaukee Area Technical College BEST program) for a fellowship.

Notes

A patent application describing compounds reported in this manuscript has been submitted. C.D. is an inventor on a patent (WO 2012/040636) containing previously reported compounds included in this paper. An earlier version of this manuscript was posted to the preprint server ChemRxiv.[33]

ACKNOWLEDGMENTS

We thank Irene Hernandez, and Trudy Holyst (Blood Research Institute) for assistance with cell culture and assay troubleshooting, Dr. Peter Newman and Dr. Huiying Zhi (Blood Research Institute) for assistance with the platelet aggregation assay, and Dr. Sheng Cai and Dennis Wiedenhoeft (Marquette University) for assistance with LC-MS and NMR instruments. We thank ACD/Labs (NMR processing) and ChemAxon (NMR prediction and compound naming and property prediction) for providing access to software. Receptor binding profiles were provided by the National Institute of Mental Health's Psychoactive Drug Screening Program, Contract # HHSN-271-2018-00023-C (NIMH PDSP). The NIMH PDSP is Directed by Bryan L. Roth MD, PhD at the University of North Carolina at Chapel Hill and Project Officer Jamie Driscoll at NIMH, Bethesda MD, USA.

ABBREVIATIONS

aPC, activated Protein C; Boc, *tert*-butoxycarbonyl; DCE, 1,2-dichloroethane; DCM, dichloromethane; DIC, disseminated intravascular coagulation; DIEA, *N,N*-diisopropylethylamine; DMAP, 4-dimethylaminopyridine; DMF, *N,N*-dimethylformamide; DMSO, dimethylsulfoxide; EDC, 1-ethyl-3-(3-dimethylaminopropyl)carbodiimide; FDA, U.S. Food and Drug Administration; GPCR, G protein coupled receptor; HATU, hexafluorophosphate azabenzotriazole tetramethyl uronium; HOBt, 1-hydroxybenzotriazole; HTS, high-throughput screening; HUVEC, human umbilical vein endothelial cells; IC_{50}, half-maximal inhibitory concentration; $i Ca^{2+}$, intracellular calcium mobilization; LC-MS, liquid chromatography-mass spectrometry; MI, myocardial infarction; NMR, nuclear magnetic resonance; PAR, protease-activated receptor; qPCR, quantitative polymerase chain reaction; SAR, structure-activity relationship; SEM, standard error of the mean; TF, tissue factor; TLC, thin layer chromatography; TNF-α, Tumor Necrosis Factor-alpha.

REFERENCES

(1) Chen, J.; Ishii, M.; Wang, L.; Ishii, K.; Coughlin, S. R. Thrombin Receptor Activation. Confirmation of the Intramolecular Tethered Liganding Hypothesis and Discovery of an Alternative Intermolecular Liganding Mode. *J. Biol. Chem.* **1994**, *269*, 16041–16045.

(2) Adams, M. N.; Ramachandran, R.; Yau, M.-K.; Suen, J. Y.; Fairlie, D. P.; Hollenberg, M. D.; Hooper, J. D. Structure, Function and Pathophysiology of Protease Activated Receptors. *Pharmacol. Ther.* **2011**, *130*, 248–282.

(3) Ramachandran, R.; Noorbakhsh, F.; DeFea, K.; Hollenberg, M. D. Targeting Proteinase-Activated Receptors: Therapeutic Potential and Challenges. *Nat Rev Drug Discov* **2012**, *11*, 69–86.

(4) Hollenberg, M. D.; Mihara, K.; Polley, D.; Suen, J. Y.; Han, A.; Fairlie, D. P.; Ramachandran, R. Biased Signalling and Proteinase-Activated Receptors (PARs): Targeting Inflammatory Disease. *British Journal of Pharmacology* **2014**, *171*, 1180–1194.

(5) Soh, U. J.; Trejo, J. Activated Protein C Promotes Protease-Activated Receptor-1 Cytoprotective Signaling Through B-Arrestin and Dishevelled-2 Scaffolds. *Proc. Natl. Acad. Sci. U.S.A.* **2011**, *108*, E1372–E1380.

(6) Madhusudhan, T.; Wang, H.; Straub, B. K.; Grone, E.; Zhou, Q.; Shahzad, K.; Muller-Krebs, S.; Schwenger, V.; Gerlitz, B.; Grinnell, B. W.; Griffin, J. H.; Reiser, J.; Grone, H. J.; Esmon, C. T.; Nawroth, P. P.; Isermann, B. Cytoprotective Signaling by Activated Protein C Requires Protease-Activated Receptor-3 in Podocytes. *Blood* **2012**, *119*, 874–883.

(7) Schuepbach, R. A.; Madon, J.; Ender, M.; Galli, P.; Riewald, M. Protease-Activated Receptor-1 Cleaved at R46 Mediates Cytoprotective Effects. *J. Thromb. Haemost.* **2012**, *10*, 1675–1684.

(8) Mosnier, L. O.; Sinha, R. K.; Burnier, L.; Bouwens, E. A.; Griffin, J. H. Biased Agonism of Protease-Activated Receptor 1 by Activated Protein C Caused by Noncanonical Cleavage at Arg46. *Blood* **2012**, *120*, 5237–5246.

(9) Bouwens, E.; Stavenuiter, F.; Mosnier, L. O. Mechanisms of Anticoagulant and Cytoprotective Actions of the Protein C Pathway. *Journal of Thrombosis and Haemostasis* **2013**, *11*, 242–253.

(10) Burnier, L.; Mosnier, L. O. Novel Mechanisms for Activated Protein C Cytoprotective Activities Involving Noncanonical Activation of Protease-Activated Receptor 3. *Blood* **2013**, *122*, 807–816.

(11) Rasmussen, U. B.; Gachet, C.; Schlesinger, Y.; Hanau, D.; Ohlmann, P.; Van Obberghen-Schilling, E.; Pouysségur, J.; Cazenave, J. P.; Pavirani, A. A Peptide Ligand of the Human Thrombin Receptor Antagonizes Alpha-Thrombin and Partially Activates Platelets. *J. Biol. Chem.* **1993**, *268*, 14322–14328.

(12) Ramachandran, R.; Mihara, K.; Mathur, M.; Rochdi, M. D.; Bouvier, M.; DeFea, K.; Hollenberg, M. D. Agonist-Biased Signaling via Proteinase Activated Receptor-2: Differential Activation of Calcium and Mitogen-Activated Protein Kinase Pathways. *Molecular Pharmacology* **2009**, *76*, 791–801.

(13) Barry, G. D.; Suen, J. Y.; Le, G. T.; Cotterell, A.; Reid, R. C.; Fairlie, D. P. Novel Agonists and Antagonists for Human Protease Activated Receptor 2. *J. Med. Chem.* **2010**, *53*, 7428–7440.

(14) Suen, J. Y.; Barry, G. D.; Lohman, R. J.; Halili, M. A.; Cotterell, A. J.; Le, G. T.; Fairlie, D. P. Modulating Human Proteinase Activated Receptor 2 with a Novel Antagonist (GB88) and Agonist (GB110). *British Journal of Pharmacology* **2012**, *165*, 1413–1423.

(15) Covic, L.; Gresser, A. L.; Talavera, J.; Swift, S.; Kuliopulos, A. Activation and Inhibition of G Protein-Coupled Receptors by Cell-Penetrating Membrane-Tethered Peptides. *Proc. Natl. Acad. Sci. U.S.A.* **2002**, *99*, 643–648.

(16) Carlson, K. E.; McMurry, T. J.; Hunt, S. W., III. Pepducins: Lipopeptide Allosteric Modulators of GPCR Signaling. *Drug Discovery Today: Technologies* **2012**, *9*, e33–e39.

(17) Zhang, P.; Leger, A. J.; Baleja, J. D.; Rana, R.; Corlin, T.; Nguyen, N.; Koukos, G.; Bohm, A.; Covic, L.; Kuliopulos, A. Allosteric Activation of a G Protein-Coupled Receptor with Cell-Penetrating Receptor Mimetics. *Journal of Biological Chemistry* **2015**, *290*, 15785–15798.

(18) Sevigny, L. M.; Zhang, P.; Bohm, A.; Lazarides, K.; Perides, G.; Covic, L.; Kuliopulos, A. Interdicting Protease-Activated Receptor-2-Driven Inflammation with Cell-Penetrating Pepducins. *Proceedings of the National Academy of Sciences* **2011**, *108*, 8491–8496.

(19) Dowal, L.; Sim, D. S.; Dilks, J. R.; Blair, P.; Beaudry, S.; Denker, B. M.; Koukos, G.; Kuliopulos, A.; Flaumenhaft, R. Identification of an Antithrombotic Allosteric Modulator That Acts Through Helix 8 of PAR1. *Proceedings of the National Academy of Sciences* **2011**, *108*, 2951–2956.

(20) Dockendorff, C.; Aisiku, O.; Verplank, L.; Dilks, J. R.; Smith, D. A.; Gunnink, S. F.; Dowal, L.; Negri, J.; Palmer, M.; Macpherson, L.; Schreiber, S. L.; Flaumenhaft, R. Discovery of 1,3-Diaminobenzenes as Selective Inhibitors of Platelet Activation at the PAR1 Receptor. *ACS Med Chem Lett* **2012**, *3*, 232–237.

(21) Aisiku, O.; Peters, C. G.; De Ceunynck, K.; Ghosh, C. C.; Dilks, J. R.; Fustolo-Gunnink, S. F.; Huang, M.; Dockendorff, C.; Parikh, S. M.; Flaumenhaft, R. Parmodulins Inhibit Thrombus Formation Without Inducing Endothelial Injury Caused by Vorapaxar. *Blood* **2015**, *125*, 1976–1985.

(22) De Ceunynck, K.; Peters, C. G.; Jain, A.; Higgins, S. J.; Aisiku, O.; Fitch-Tewfik, J. L.; Chaudhry, S. A.; Dockendorff, C.; Parikh, S. M.; Ingber, D. E.; Flaumenhaft, R. PAR1 Agonists Stimulate APC-Like Endothelial Cytoprotection and Confer Resistance to Thromboinflammatory Injury. *Proceedings of the National Academy of Sciences* **2018**, *115*, E982–E991.

(23) Nazir, S.; Gadi, I.; Al-Dabet, M. M.; Elwakiel, A.; Kohli, S.; Ghosh, S.; Manoharan, J.; Ranjan, S.; Bock, F.; Braun-Dullaeus, R. C.; Esmon, C. T.; Huber, T. B.; Camerer, E.; Dockendorff, C.; Griffin, J. H.; Isermann, B.; Shahzad, K. Cytoprotective Activated Protein C Averts Nlrp3 Inflammasome Induced Ischemia Reperfusion Injury via mTORC1 Inhibition. *Blood* **2017**, *130*, 2664–2677.

(24) Gandhi, D. M.; Majewski, M. W.; Rosas, R.; Kentala, K.; Foster, T. J.; Greve, E.; Dockendorff, C. Characterization of Protease-Activated Receptor (PAR) Ligands: Parmodulins Are Reversible Allosteric Inhibitors of PAR1-Driven Calcium Mobilization in Endothelial Cells. *Bioorganic & Medicinal Chemistry* **2018**, *26*, 2514–2529.

(25) Mosnier, L. O.; Griffin, J. H. Inhibition of Staurosporine-Induced Apoptosis of Endothelial Cells by Activated Protein C Requires Protease-Activated Receptor-1 and Endothelial Cell Protein C Receptor. *Biochem. J.* **2003**, *373*, 65–70.

(26) Verplank, L.; Dockendorff, C.; Negri, J.; Perez, J. R.; Dilks, J.; Macpherson, L.; Palmer, M.; Flaumenhaft, R.; Schreiber, S. L. *Chemical Genetic Analysis of Platelet Granule Secretion-Probe 3*; National Center for Biotechnology Information (US): Bethesda (MD), 2010. http://www.ncbi.nlm.nih.gov/books/NBK55066/

(27) Chu, A. J. Tissue Factor Mediates Inflammation. *Arch. Biochem. Biophys.* **2005**, *440*, 123–132.

(28) Bevilacqua, M. P.; Pober, J. S.; Majeau, G. R.; Fiers, W.; Cotran, R. S.; Gimbrone, M. A. Recombinant Tumor Necrosis Factor Induces Procoagulant Activity in Cultured Human Vascular Endothelium: Characterization and Comparison with the Actions of Interleukin 1. *Proc. Natl. Acad. Sci. U.S.A.* **1986**, *83*, 4533–4537.

(29) Nawroth, P. P.; Stern, D. M. Modulation of Endothelial Cell Hemostatic Properties by Tumor Necrosis Factor. *J. Exp. Med.* **1986**, *163*, 740–745.

(30) Colucci, M.; Balconi, G.; Lorenzet, R.; Pietra, A.; Locati, D.; Donati, M. B.; Semeraro, N. Cultured Human Endothelial Cells Generate Tissue Factor in Response to Endotoxin. *Journal of Clinical Investigation* **1983**, *71*, 1893–1896.

(31) Gando, S.; Levi, M.; Toh, C.-H. Disseminated Intravascular Coagulation. *Nat Rev Dis Primers* **2016**, *2*, 16037.

(32) Besnard, J.; Ruda, G. F.; Setola, V.; Abecassis, K.; Rodriguiz, R. M.; Huang, X.-P.; Norval, S.; Sassano, M. F.; Shin, A. I.; Webster, L. A.; Simeons, F. R. C.; Stojanovski, L.; Prat, A.; Seidah, N. G.; Constam, D. B.; Bickerton, G. R.; Read, K. D.; Wetsel, W. C.; Gilbert, I. H.; Roth, B. L.; Hopkins, A. L. Automated Design of Ligands to Polypharmacological Profiles. *Nature* **2012**, *492*, 215–220.

(33) Gandhi, D.; Rosas, R., Jr; Greve, E.; Kentala, K.; Diby, N.; Snyder, V. A.; Stephans, A.; Yeung, T.; Subramaniam, S.; Kurtenbach, K.; DiMilo, E.; Arnold, L.; Weiler, H.; Dockendorff, C. The Parmodulin NRD-21 Is an Allosteric Inhibitor of PAR1 Gq Signaling with Improved Anti-Inflammatory Activity and Stability. *ChemRxiv (preprint)* **2019**. https://doi.org/10.26434/chemrxiv.7755479.v1